Japanese Journal of Applied Physics **53**, 031301 (2014) **REGULAR PAPER**
http://dx.doi.org/10.7567/JJAP.53.031301

Photo induced minority carrier annihilation at crystalline silicon surface in metal oxide semiconductor structure

Toshiyuki Sameshima*, Jun Furukawa, Tomohiko Nakamura, Satoshi Shigeno, Tomohito Node, Shinya Yoshidomi, and Masahiko Hasumi

Faculty of Engineering, Tokyo University of Agriculture and Technology, Koganei, Tokyo 184-8588, Japan
E-mail: tsamesim@cc.tuat.ac.jp

Received August 22, 2013; accepted December 2, 2013; published online February 12, 2014

We report the properties of features of photo induced minority carrier annihilation at the silicon surface in a metal–oxide–semiconductor (MOS) structure using 9.35 GHz microwave transmittance measurement. 7 Ω cm n-type 500-μm-thick crystalline silicon substrates coated with 100-nm-thick thermally grown SiO_2 layers were prepared. Part of the SiO_2 at the rear surface was removed. Al electrode bars were formed at the top and rear surfaces to form the structures Al/SiO_2/Si/SiO_2/Al and Al/SiO_2/Si/Al. 635 nm light illumination onto the top surface caused photo induced carriers to be in one side of the silicon region of the Al electrode bar of the structure Al/SiO_2/Si/SiO_2/Al. Microwave transmittance was measured on the other side of the silicon region of the Al electrode bars. The measurement and analysis of microwave absorption by photo induced carriers laterally diffusing across the silicon region coated with Al electrodes revealed a change in the carrier recombination velocity at the silicon surface with the bias voltage applied onto the top Al electrode. The applied bias voltages of +2.0 and −2.2 V gave peaks at surface recombination velocities of 83 and 86 cm/s, respectively, for the sample structure Al/SiO_2/Si/SiO_2/Al, while it was 44 cm/s under the bias-free condition. A peak surface recombination velocity of 81 cm/s was only observed at a bias voltage of −2.0 V for the sample structure Al/SiO_2/Si/Al.
© 2014 The Japan Society of Applied Physics

1. Introduction

A long lifetime of photo induced minority carriers is required for fabricating high-performance photosensors[1–5] and photovoltaic devices.[1,6–9] Carrier recombination defect states seriously affect the minority carrier effective lifetime of silicon[10–19] and mainly concentrate at the silicon surface or its interface. A metal–oxide–semiconductor (MOS) structure is essential for semiconductor devices.[20] The application of a bias voltage onto metal electrodes causes band bending and changes in the carrier concentration of the silicon surface region that satisfy the charge neutrality between both sides of the oxide insulating layer. The oxide layer also plays a role in surface passivation through the termination of dangling bonds of silicon. The photo induced carrier recombination defect density and recombination velocity are low at the oxide layer/silicon interface in general. Because the bias voltage changes the occupation probability of surface defect states, the photo induced carrier recombination probability depends on the bias voltage. The capacitance response with an alternative voltage as a function of the bias voltage (C–V) has been widely used to estimate the surface potential as a function of the bias voltage and the density of carrier traps at the silicon interface for MOS capacitors in a dark field.[20] The direct measurement of photo induced carrier recombination probability as a function of bias voltage will give useful information for fabricating high-performance photosensors and passivation layers for photovoltaic devices.

In this paper, we report the measurement of the light-induced excess carrier recombination velocity at the silicon surface in the MOS structure using a 9.35 GHz microwave transmittance measurement system with continuous wave (CW) light illumination.[21–24] We demonstrate a change in the microwave absorption of photo induced carriers laterally diffused in the silicon region of the MOS structure with the application of bias voltage. Analysis of the experimental results shows that bias voltage application causes a change in the carrier recombination velocity.

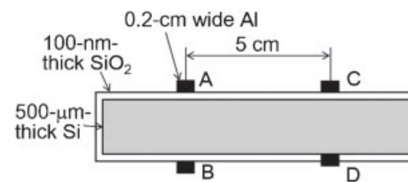

Fig. 1. Schematic cross section of the sample. The area of Al electrodes was 0.2 × 4.0 cm^2.

2. Experimental procedure

N-type crystalline silicon substrates with an orientation of (100) and a thickness of 500 μm were prepared. Their top and rear surfaces were coated with 100-nm-thick thermally grown SiO_2 layers. The SiO_2 layer was etched out using hydrofluoric acid in a small region with an area of 0.2 × 4.0 cm^2 at the rear surface, as shown in the schematic cross section in Fig. 1. Two sets of 100-nm-thick Al electrodes with a size of 0.2 × 4.0 cm^2 were then formed in parallel with a distance of 5.0 cm on the top and bottom surfaces each by vacuum evaporation. They are named A–D, as shown in Fig. 1. Al electrodes A and B, and C and D faced each other in the same horizontal position. The Al electrode D was formed directly on the silicon surface where SiO_2 was removed.

A 9.35 GHz microwave transmittance measurement system was used in order to detect the photo induced minority carriers of the samples, as shown in Fig. 2(a). The system had waveguide tubes, which had a narrow gap. Each sample was placed in the gap between the waveguide tubes. Two modes of CW 635 nm laser diode light illumination were used for the present purpose. First, CW 635 nm light was introduced in the waveguide tube with a cross section of 1.0 × 2.3 cm^2 and illuminated onto the sample surface over the entire area in the tube when Al electrodes A and B were coincidentally positioned on the 0.2-cm-thick wall of the waveguide tubes, as shown in Fig. 2(a). The light intensity was set at 1.5

 © 2014 The Japan Society of Applied Physics

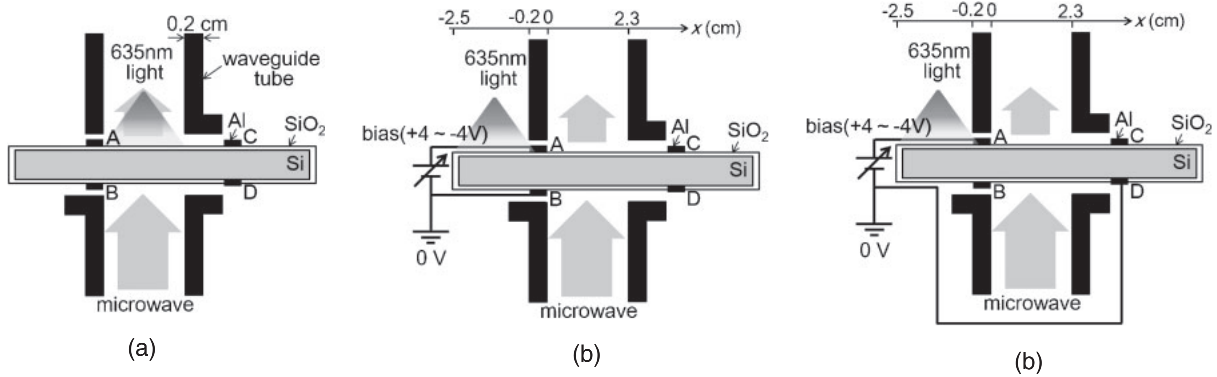

Fig. 2. 9.35 GHz microwave transmittance measurement with CW 635 nm laser diode light introduced in the waveguide tubes (a), light was illuminated to the outside silicon region of the waveguide tube and the bias voltage was applied to electrode A while keeping electrode B at the rear surface at 0 V (b), and the bias voltage was applied to electrode A while keeping electrode D at the rear surface at 0 V (c). The horizontal distance was also plotted with zero at the internal edge of the waveguide tube in (b) and (c).

mW/cm^2 at the sample surface. Photo induced carriers were generated in the 3 µm surface region by 635 nm light absorption.[25] The microwave transmissivities of the sample in the dark, T_d, and under light illumination, T_p, were measured for duration of 4 s each.[21] T_d gave the electrical resistivity, the majority carrier density of electrons and the Fermi level. The logarithmic ratio of $\ln(T_d/T_p)$ is proportional to the density of minority carriers per unit area, N. Because N is given by the effective minority carrier lifetime τ_{eff} and the carrier generation rate G per unit area as[21,23]

$$N = \tau_{eff} \times G. \quad (1)$$

Here, τ_{eff} is determined by $\ln(T_d/T_p)$. The uncertainty coefficients between $\ln(T_d/T_p)$ and N were determined by the method of microwave absorption under multiply periodic pulsed light illumination,[23] which gave τ_{eff} independently of the effective loss of the optical reflectivity, which depends on the incident angle of light and the surface structure in general.

The other mode of CW 635 nm light illumination onto the outside of the waveguide tube was conducted, as shown in Fig. 2(b). Photo induced carriers generated at the surface region diffuse in the lateral direction as well as in the depth direction. If τ_{eff} is long enough, photo induced carriers traverse under the 0.2-cm-thick wall of the waveguide tube and diffuse into the region of microwave absorption measurement. Photo induced carriers that laterally diffused into the region in the waveguide tube via the region covered with the Al electrodes were observed with microwave absorption. $\ln(T_d/T_p)$ was measured by turning the CW 635 nm light ON and OFF. Moreover, the microwave absorption measurement was carried out by applying a bias voltage from −4 to 4 V to electrode A at the top surface and keeping electrode B at the rear surface at 0 V. Each bias voltage was maintained for 10 s, in which T_d was measured for 4 s at 2 s from the bias voltage application and T_p was subsequently measured for 4 s in order to realize measurement in the electrically steady state. The same $\ln(T_d/T_p)$ was obtained in the cases of the free and 0 V biases. Although electrodes A and B were formed on the SiO_2 layers and the silicon surfaces were not directly electrically biased, the band bending of the silicon surface regions occured to achieve balance among the applied voltage, the silicon surface potential, and the voltage applied to the SiO_2 layers. The electron accumulation in the surface region under electrode A will occur with a positive bias voltage application to electrode A. On the other hand, the electron depletion or hole accumulation will be induced by a negative bias voltage application to electrode A.

Photo induced carrier microwave absorption was also measured when the bias voltage in the range from −4 to 4 V was applied to electrode A at the top surface while keeping electrode D at 0 V, as shown in Fig. 2(c). Each bias voltage was maintained for 10 s, in which T_d was measured for 4 s from 2 s after the bias voltage application and T_p was subsequently measured for 4 s. Because electrode D was directly formed on the silicon surface, the sample with electrodes A and D had a conventional MOS structure. The distance of 5.0 cm between the two electrodes was much larger than the carrier diffusion length.[24] This configuration of electrodes allows photo induced carrier microwave absorption measurement with no effect of substantial carrier recombination at the interface of silicon and electrode D.

The *C*–*V* characteristics at the 100 kHz alternative voltage with an amplitude of 10 mV as a function of bias voltage were measured in a dark field for the sample with electrodes A and B to investigate the formation of carrier depletion layers associated with bias-induced band bending. The 100 kHz alternative probe voltage and bias voltage were applied to electrode A, while 0 V was applied to electrode B. The Al electrodes were large with a strip shape, which were very different from the conventional small dot-type electrodes used in *C*–*V* measurements. To avoid a spatial voltage change in the electrodes, a low frequency of 100 kHz was selected as the probe frequency. Each bias voltage was maintained for 4 s in order to realize measurement in the electrically steady state. For comparison with those of the sample with electrodes A and B, the *C*–*V* characteristics of the sample with electrodes C and D were measured in a dark field, as shown in Fig. 1. The 100 kHz alternative voltage and bias voltage were applied to electrode C at the top surface, while 0 V was applied to electrode D. Each bias voltage was maintained for 4 s. The samples with electrodes C and D had the same structural configuration as those with electrodes A and B, except for electrode D directly contacting at the silicon surface.

 © 2014 The Japan Society of Applied Physics

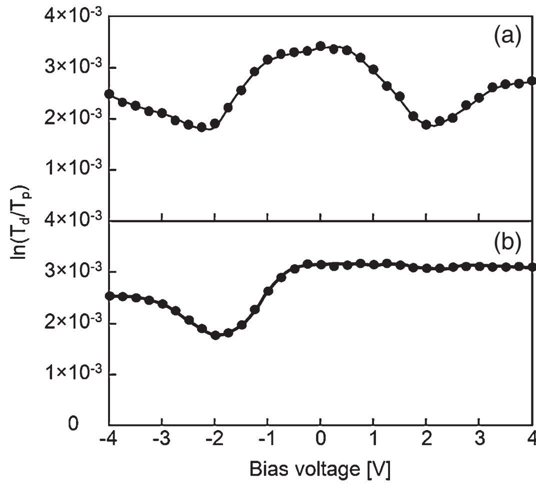

Fig. 3. $\ln(T_d/T_p)$ as a function of bias voltage in the cases of microwave absorption measurements with light illumination outside of the waveguide tubes while biasing electrode A and keeping electrode B at 0 V (a), and while biasing electrode A and keeping electrode D at 0 V (b).

3. Results and discussion

The measurements of T_d and T_p using the system shown in Fig. 2(a) gave a resistivity, a majority electron carrier density, a Fermi level from the valence band top, and τ_{eff} of 7 Ω cm, 6.0×10^{14} cm^{-3}, 0.856 eV, and 1.1×10^{-3} s, respectively, which were obtained through light illumination in the waveguide tube. If the bulk lifetime τ_b is large enough, τ_{eff} is governed by the same surface recombination velocity located at the surface. The total recombination velocity S_T at the top and rear surfaces was obtained as 44 cm/s, determined by our analysis program.[22] Using the Fitzgerald formula under the flat band condition,[26] S_T proportionally gave a total density of surface recombination defects of 2.8×10^{10} cm^{-2}, including at the top and rear surfaces. The silicon surfaces were well passivated by thermally grown SiO_2 under the bias-free condition. The effective minority hole carrier diffusion length L was estimated as 0.115 cm, which was given by the product of τ_{eff} and the diffusion coefficient. This large L indicates that the photo induced excess minority carriers diffused over the entire substrate thickness and over a long horizontal distance.

Figure 3 shows $\ln(T_d/T_p)$ as a function of the bias voltage in the cases of microwave absorption measurements with light illumination outside of the waveguide tubes with biased between (a) A and B, and (b) A and D electrodes. $\ln(T_d/T_p)$ was 3.4×10^{-3} at 0 V in the bias case of electrodes A and B, as shown in Fig. 3(a), which was the same as that in the open-circuit case. We interpret the generation of photo induced minority carriers by 635 nm light illumination diffused in the lateral direction into the area of the waveguide tube with an initial τ_{eff} of 1.1×10^{-3} s at a bias voltage of 0 V. An approximately symmetrical curve of $\ln(T_d/T_p)$ as a function of the bias voltage was obtained, as shown in Fig. 3(a). $\ln(T_d/T_p)$ decreased from 3.4×10^{-3} to 1.9×10^{-3} as the bias voltage increased from 0 to +2.0 V and decreased to 1.8×10^{-3} as the bias voltage decreased to −2.2 V. This indicates that carrier annihilation rate in the region covered with the Al electrode was increased by the bias voltage application to +2 V. On the other hand, $\ln(T_d/T_p)$ increased again to 2.7×10^{-3} and 2.5×10^{-3} as the bias voltage further increased to +4 V and decreased to −4 V, respectively. This means that the carrier annihilation rate in the region underlying the Al electrode became low again at a high bias voltage. For the bias between electrodes A and D, an approximately step like curve of $\ln(T_d/T_p)$ was obtained, as shown in Fig. 3(b). $\ln(T_d/T_p)$ decreased from 3.2×10^{-3} to 1.8×10^{-3} as the bias voltage decreased from 0 to −2.0 V. It again increased to 2.5×10^{-3} as the bias voltage further decreased to −4.0 V. On the other hand, positive bias application hardly changed $\ln(T_d/T_p)$.

In order to analyze the result of Fig. 3, a numerical analysis program of carrier diffusion and annihilation using the finite differential element method was constructed. In the simple carrier diffusion model, the surface recombination velocity was programmed to be variable for the region of MOS structure. The photo induced minority carrier density $N(x, y)$ as a function of the lateral position x and the depth position y from the top surface is given using the carrier diffusion model under a two-dimensional steady-state condition as[27,28]

$$D\frac{\partial^2 N(x,y)}{\partial x^2} + D\frac{\partial^2 N(x,y)}{\partial y^2} - \frac{N(x,y)}{\tau_b} + g(x,y) = 0 \quad (2a)$$

$$D\frac{\partial N(x,y)}{\partial y}\bigg|_{y=0} = S_{top}N(x,0) - g(x,0)\Delta y \quad (2b)$$

$$D\frac{\partial N(x,y)}{\partial y}\bigg|_{y=d} = -S_{rear}N(x,d) + g(x,d)\Delta y \quad (2c)$$

where D is the diffusion coefficient of the minority carrier, τ_b is the bulk lifetime assumed to be large at 0.01 s, S_{top} is the carrier recombination velocity at the top surface, S_{rear} is the carrier recombination velocity at the rear surface, d is the substrate thickness of 500 µm, $g(x, y)$ is the carrier generation rate, and Δy is the lattice unit in the depth direction of 20 µm, which was set much lower than the effective carrier diffusion length of 0.115 cm. The lattice unit in the horizontal direction, Δx, was also set at 20 µm. Calculation boundary conditions were placed corresponding to the experimental configuration, as shown in Fig. 4(a). $g(x, y)$ was only set as a constant of g at the x position lower than −0.2 cm and at the first lattice of the depth for carrier generation at the surface outside of the waveguide tube. Since the experimental τ_{eff} of 1.1×10^{-3} s for the bias-free sample gave S_T of 44 cm/s ($= S_{top} + S_{rear}$), in the regions with x lower than −0.2 cm or larger than 0 cm, S_{top} and S_{rear} were set at 22 cm/s. S_{top} and S_{rear} were programmed to be variable for x between −0.2 and 0 cm corresponding to the region covered with Al electrodes. The total minority carrier number N_T in the region where the microwave transmitted the sample was then calculated by integrating $N(x, y)$ with respect to y from 0 to d and to x from 0 to 2.3 cm (the length of the microwave tube), as shown by the image in the lateral direction in Fig. 4(b). $\ln(T_d/T_p)$ was calculated from N_T using the free-carrier microwave absorption theory.[21,23] The most possible S_T ($= S_{top} + S_{rear}$) in the region with x between −0.2 and 0 cm was determined by fitting the calculated $\ln(T_d/T_p)$ values to the experimental ones shown in Fig. 3 within the accuracy of the present numerical analysis with the lattice unit.

 © 2014 The Japan Society of Applied Physics

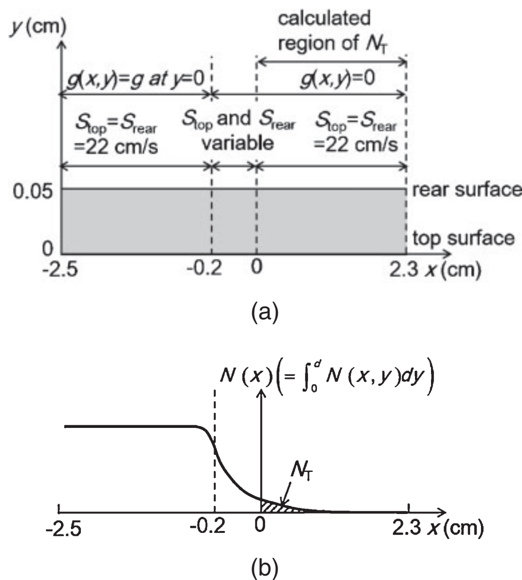

Fig. 4. Two-dimensional numerical calculation model of photo induced carrier diffusion in the lateral x- and depth y-directions (a) and image of carrier concentration distribution in the x-direction giving N_T (b).

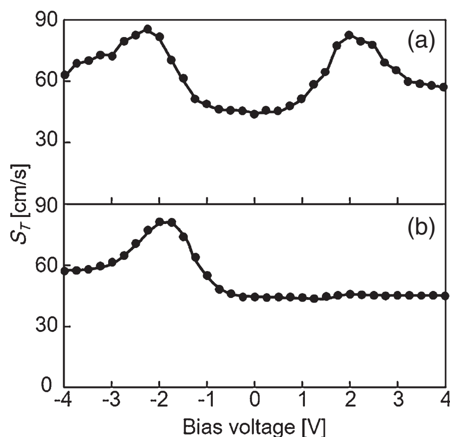

Fig. 5. S_T analyzed from the experimental result of Fig. 3 as a function of the voltage biased for electrodes A while keeping electrode B at 0 V (a), and for electrode A while keeping electrode D at 0 V (b).

Figure 5 shows the S_T analyzed from the experimental results in Fig. 3 as a function of the voltage biased between electrodes of A and B (a), and A and D (b). S_T symmetrically changed with the bias voltage in the case of bias voltage application to electrodes A and B, as shown in Fig. 5(a). It increased from 44 to 83 cm/s as the bias voltage increased from 0 to +2.0 V. It also increased to 86 cm/s as the bias voltage decreased to −2.2 V. On the other hand, S_T decreased to 57 cm/s as the bias voltage further increased to +4 V. It decreased again to 63 cm/s as the bias voltage further decreased to −4 V. An asymmetric characteristic in S_T was obtained in the case of bias at the electrodes A and D, as shown in Fig. 5(b). S_T increased from 44 to 81 cm/s as the bias voltage decreased from 0 to −2.0 V. It decreased again to 57 cm/s as the bias voltage further decreased to −4.0 V. On the other hand, a positive bias of up to +2.0 V hardly changed S_T.

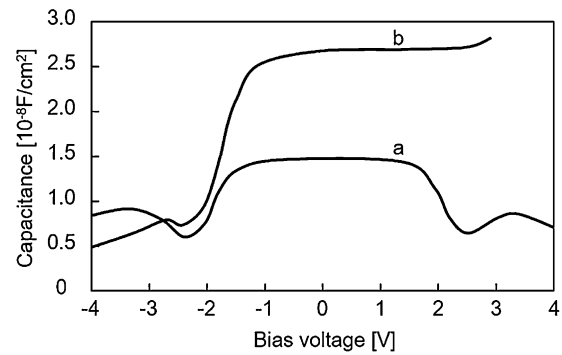

Fig. 6. C–V characteristics at 100 kHz as a function of bias voltage in the range from −4 to 4 V when the bias and 100 kHz probe voltage were applied to the electrode A with keeping electrode B at 0 V (curve a) and to electrode C while keeping electrode D at 0 V (curve b).

Figure 6 shows the C–V characteristics at 100 kHz as a function of the bias voltage in the range from −4 to 4 V when the bias and 100 kHz probe voltage were applied to electrode A while keeping electrode B at 0 V (curve a) and applied to electrode C while keeping electrode D at 0 V (curve b). A symmetrical curve of C–V was obtained in the case of voltage application between electrodes A and B. The capacitance almost leveled off with 1.5×10^{-8} F/cm^2 at 0 V. It corresponds to the effective capacitance of the series connected oxide capacitors of the top and bottom SiO_2 layers with the structure Al/SiO_2/Si/SiO_2/Al. The capacitance markedly decreased as the voltage increased from 1.5 to 2.4 V or decreased from −1.4 to −2.3 V. This means that the capacitance of the depletion layer was formed in the top or rear surface regions by negative or positive voltage application. On the other hand, the capacitance was 2.7×10^{-8} F/cm^2 at 0 V in the case of bias voltage application between the electrodes C and D. This resulted from the oxide capacitances of the top SiO_2 layer with the structure Al/SiO_2/Si/Al. The capacitance only decreased as the bias voltage decreased. This characteristic shows that the top silicon surface region covered with electrode C was depleted by the negative bias voltage application. The analysis of the C–V curve using the conventional method[20] in the case of voltage application between the electrodes C and D gave a flat band voltage, a voltage for the Fermi level at the surface positioning at the mid gap, and a threshold voltage of the inversion mode at the top surface of −1.6, −2.1, and −2.7 V, respectively. The analysis also resulted in a density of carrier traps at the top surface of 6.0×10^{10} cm^{-2} eV^{-1} at the mid gap.

The results in Fig. 3 show that the total density of minority carriers, N_T, that traversed from the light illumination region to the microwave absorption measurement region shown in Figs. 2 and 4 decreased and showed valleys with bias application at +2.0 and −2.2 V for the sample structure Al/SiO_2/Si/SiO_2/Al, and that N_T decreased and showed a valley with bias application only at −2.0 V for the sample structure Al/SiO_2/Si/Al. The numerical analysis with the simple carrier diffusion model with a variable surface recombination velocity revealed that the decrease in N_T was caused by increase in S_T, as shown in Fig. 5. When a positive bias voltage is applied to electrode A for the sample structure Al/SiO_2/Si/SiO_2/Al, the surface potential at the silicon top

© 2014 The Japan Society of Applied Physics

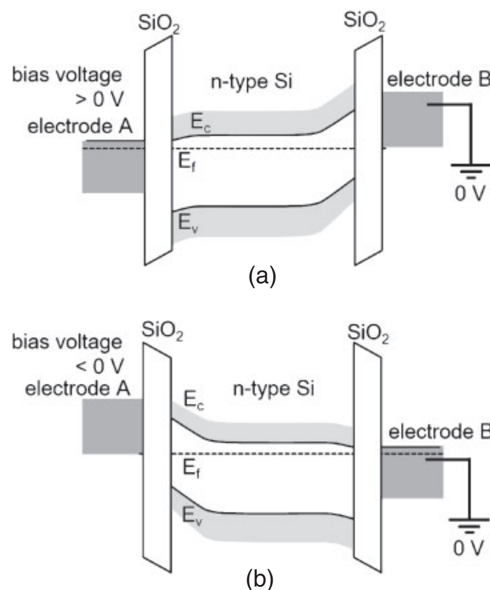

Fig. 7. Schematic band bending image when a positive bias voltage is applied to electrode A (a) and a negative bias voltage is applied to electrode A (b).

surface below electrode A decreases and an electron-accumulating region is formed, as shown by the band bending image in Fig. 7(a). In contrast, the surface potential at the silicon rear surface above electrode B moves up and electron depleted region is formed at the rear surface. On the other hand, the negative bias voltage application causes the opposite situation with electron depleting at the top surface and electron accumulating at the rear surface, as shown in Fig. 7(b). The marked decreases in the capacitance in the *C–V* characteristics shown in Fig. 6 indicate that the two peaks of S_T shown in Fig. 5(a) appeared at the carrier depleted condition at the top or rear surfaces. In the case of the present sample with the majority carrier density of $6.0 \times 10^{14}\,cm^{-3}$, the length of the carrier depletion region is estimated as 1.2 µm, which is much lower than the minority carrier diffusion length. The small length of the carrier depletion region means that light-induced excess carriers diffused under the bias-free condition of in the almost entire silicon region. However, when light-induced excess minority carriers traverse at the carrier depletion edge near the silicon surface, minority carriers will be accelerated toward the silicon surface owing to the attractive potential slope. Carrier recombination will be promoted by minority carrier injection into the surface associated with the potential slope in the carrier depletion region.[27,28] The density of the surface minority carriers at the silicon surface will therefore decrease. The results of S_T shown in Fig. 5 suggest that the density of minority carrier at the silicon surface decreased to about 50% of the initial density under the bias-free condition, if the density of recombination defect states and capture cross section are not changed from the initial values with bias free. On the other hand, the location of the Fermi level at the midgap at the silicon surface by the bias application can increase the inoccupation probability of defects. There is a possibility of increasing in the density of recombination defect states. The present measurement method will give useful experimental data for the analysis of carrier annihilation properties at the MOS interface. In the case of the sample structure $Al/SiO_2/Si/Al$, positive bias voltage application will induce electron accumulation at the top silicon surface. The field effect passivation is therefore expected as is widely reported.[29–31] The results in Fig. 5(b) showed that S_T almost leveled off as a function of bias voltage from 0 to +4 V. The field effect passivation was not observed in this sample.

The results in Figs. 3–5 show that the present method makes it possible to precisely measure surface carrier recombination properties, which depend on bias voltage. This method will be applicable for the investigation of the carrier annihilation properties of a semiconductor interface with bias for different passivation materials such as SiN and HfO_2.

4. Conclusions

We reported the features of photo induced minority carrier annihilation properties at the silicon surface in a MOS structure using a 9.35 GHz microwave transmittance measurement system. 7 Ω cm n-type 500-µm-thick crystalline silicon substrates coated with 100-nm-thick thermally grown SiO_2 layers were prepared. The initial samples had τ_{eff} and S_T of 1.1×10^{-3} s and 44 cm/s, respectively. Two sets of 100-nm-thick Al electrodes A and C, and B and D with a size of $0.2 \times 4.0\,cm^2$ were formed in parallel, with a distance of 5 cm on the top and bottom surfaces, respectively. Electrode D was formed directly on the silicon surface where SiO_2 was removed. We observed $\ln(T_d/T_p)$ as a function of the bias voltage applied between electrodes A and B with the structure $Al/SiO_2/Si/SiO_2/Al$, and A and D with the structure $Al/SiO_2/Si/Al$ with light illumination outside of the waveguide tubes. The change in S_T with the bias voltage was estimated from the experimental $\ln(T_d/T_p)$ by the two dimensional numerical finite different element analysis with a lattice unit of 20 µm. S_T increased from 44 to 83 cm/s as the bias voltage increased from 0 to +2.0 V for the sample with the structure $Al/SiO_2/Si/SiO_2/Al$. It also increased to 86 cm/s as the bias voltage decreased to −2.2 V. The 100 kHz *C–V* measurements indicate that peaks of S_T occurred under the carrier depletion condition at the top or rear surface. On the other hand, in the case of the sample with the structure $Al/SiO_2/Si/Al$, S_T increased from 44 to 81 cm/s as the bias voltage decreased from 0 to −2.0 V. However, a positive bias of up to +2.0 V hardly changed S_T. Under this sample condition, the electron depletion condition only appeared in the top silicon surface region below electrode A by negative bias voltage because the silicon rear surface was biased at 0 V by electrode D. Those results show that the present method makes it possible precisely measure surface recombination properties, which depend on bias voltage.

Acknowledgments

This work was partly supported by a Grant-in-Aid for Science Research C (Nos. 25420282 and 23560360) from the Ministry of Education, Culture, Sports, Science and Technology of Japan, and Sameken Co., Ltd.

1) S. M. Sze, *Semiconductor Devices* (Wiley, New York, 1985) Chap. 7.
2) E. A. G. Webster, L. A. Grant, and R. K. Henderson, IEEE Trans. Electron Devices **60**, 1188 (2013).
3) S. E. Bohndiek, A. T. Clark, A. Blue, V. O'Shea, J. P. Crooks, C. D.

 © 2014 The Japan Society of Applied Physics

Arvanitis, G. J. Royle, M. L. Prydderch, R. Turchetta, and R. D. Speller, Opt. Eng. **46**, 124003 (2007).
4) E. A. G. Webster, L. A. Grant, and R. K. Henderson, IEEE Electron Device Lett. **33**, 1589 (2012).
5) C. D. Arvanitis, S. E. Bohndiek, G. Royle, A. Blue, H. X. Liang, A. Clark, M. Prydderch, R. Turchetta, and R. Speller, Med. Phys. **34**, 4612 (2007).
6) A. Rohatagi, Proc. 3rd World Conf. Photovoltaic Energy Conversion, 2003, A29.
7) M. A. Green, Prog. Photovoltaics **17**, 183 (2009).
8) M. A. Green, K. Emery, Y. Hishikawa, W. Warta, and E. D. Dunlop, Prog. Photovoltaics **20**, 12 (2012).
9) J. Zhao, A. Wang, M. A. Green, and F. Ferrazza, Appl. Phys. Lett. **73**, 1991 (1998).
10) G. S. Kousik, Z. G. Ling, and P. K. Ajmera, J. Appl. Phys. **72**, 141 (1992).
11) J. M. Borrego, R. J. Gutmann, N. Jensen, and O. Paz, Solid-State Electron. **30**, 195 (1987).
12) G. W. 't Hooft, C. van Opdorp, H. Veenvliet, and A. T. Vink, J. Cryst. Growth **55**, 173 (1981).
13) H. Daio and F. Shimura, Jpn. J. Appl. Phys. **32**, L1792 (1993).
14) J. Sritharathikhun, C. Banerjee, M. Otsubo, T. Sugiura, H. Yamamoto, T. Sato, A. Limmanee, A. Yamada, and M. Konagai, Jpn. J. Appl. Phys. **46**, 3296 (2007).
15) Y. Takahashi, J. Nigo, A. Ogane, Y. Uraoka, and T. Fuyuki, Jpn. J. Appl. Phys. **47**, 5320 (2008).
16) M. Boulou and D. Bois, J. Appl. Phys. **48**, 4713 (1977).
17) Y.-I. Ogita, J. Appl. Phys. **79**, 6954 (1996).
18) C. Munakata, Jpn. J. Appl. Phys. **43**, L1394 (2004).
19) K. Sakamoto and T. Sameshima, Jpn. J. Appl. Phys. **39**, 2492 (2000).
20) Y. Taur and T. Ning, *Fundamental of Modern VLSI Physics* (Cambridge University Press, Cambridge, U.K., 1998) Chap. 2.
21) T. Sameshima, H. Hayasaka, and T. Haba, Jpn. J. Appl. Phys. **48**, 021204 (2009).
22) T. Sameshima, R. Ebina, K. Betsuin, Y. Takiguchi, and M. Hasumi, Jpn. J. Appl. Phys. **52**, 011801 (2013).
23) T. Sameshima, T. Nagao, S. Yoshidomi, K. Kogure, and M. Hasumi, Jpn. J. Appl. Phys. **50**, 03CA02 (2011).
24) T. Sameshima, J. Furukawa, and S. Yoshidomi, Jpn. J. Appl. Phys. **52**, 041303 (2013).
25) E. D. Palk, *Handbook of Optical Constants of Solids* (Academic Press, London, 1985) p. 547.
26) D. J. Fitzgerald, Proc. IEEE **54**, 1601 (1966).
27) A. S. Groove, *Physics and Technology of Semiconductor Devices* (Wiley, New York, 1967) Chap. 5.
28) W. Shockley and W. T. Read, Jr., Phys. Rev. **87**, 835 (1952).
29) S. W. Glunz, A. B. Sproul, W. Warta, and W. Wettling, J. Appl. Phys. **75**, 1611 (1994).
30) S. W. Glunz, D. Biro, S. Rein, and W. Warta, J. Appl. Phys. **86**, 683 (1999).
31) R. Hezel and K. Jaeger, J. Electrochem. Soc. **136**, 518 (1989).

© 2014 The Japan Society of Applied Physics